Constrained unscented Kalman filter for parameter identification of structural systems

Dan Li [1], Yang Wang [2, 3, *]
[1] Department of Civil and Environmental Engineering, Southeast University, Nanjing, China
[2] School of Civil and Environmental Engineering, Georgia Institute of Technology, Atlanta, GA
[3] School of Electrical and Computer Engineering, Georgia Institute of Technology, Atlanta, GA
*yang.wang@ce.gatech.edu

Abstract: The unscented Kalman filter (UKF) can be used to identify model parameters of structural systems from the measurement data. However, the standard UKF may provide unreliable and non-physical estimates, since no parameter constraints are incorporated in the identification process. This paper discusses and compares several constrained UKF (CUKF) methods for parameter identification of structural systems. The effectiveness and robustness of the methods are evaluated through numerical simulation on a Bouc-Wen hysteretic system. The results demonstrate that with properly handling of the constraints, the identification accuracy can be improved. The proposed CUKF method is further validated using experimental data collected from a full-scale reinforced concrete structure. Based on the identified model parameters, the updated models can achieve more accurate simulation responses than the initial model.

Keywords: unscented Kalman filter, parameter constraints, online identification, full-scale experiment, dynamic analysis

1 Introduction

In civil engineering, finite element (FE) models are widely used to simulate behaviors of structures and provide guidance for design and maintenance. The validity of an FE model depends on the suitable values of model parameters. In practice, however, there are always uncertain material properties and boundary conditions in constructed structures. As a result, nominal property values and model simplification are usually adopted, causing inaccurate and unreliable simulation results. With the increasing availability of field measurements from constructed structures, opportunities have risen for the development of identification techniques which can tune model parameters toward providing more reliable simulation results [1]. Besides improving simulation performance, parameter identification techniques also find extensive application in structural health monitoring (SHM). Structural damages would result in changes of material properties, especially reduction of stiffness. By identifying stiffness parameters over time, structural damages, even some hardly noticeable ones, can be detected and the identification results may help evaluating condition of structures [2, 3].

Experimentally measured data serve as the baseline for structural system identification. The development of sensing technology has facilitated the implementation of vibration experiments, from which dynamic responses of structures can be measured. Various algorithms have been developed for identifying model parameters from the dynamic responses, which provide relevant information regarding the structural properties of interest (e.g. stiffness, damping and mass). Among these parameter identification algorithms, the nonlinear extensions of Kalman filter, especially the extended Kalman filter (EKF) and the unscented Kalman filter (UKF), have attracted attention from researchers due to low computational complexity and broad applicability. Treated as augmented states, model parameters can be estimated together with the original system states through the measurement data. Based on Gaussian assumption, the EKF and the UKF efficiently propagates the state estimate and covariance, and provide an approximately optimal estimation. The EKF linearizes both the dynamic equation and measurement equation using Taylor series expansion, and recursively updates the states and parameters through the linearized system. EKF based structural parameter identification has been extensively reported [4-10]. The EKF performs well for structures with mild nonlinearity but encounters challenges for highly nonlinear structures due to large error caused by linearization [11].

As a powerful alternative to the EKF, the UKF has also been investigated and applied on parameter identification for structural systems. The UKF propagates the first two moments of the states and parameters based on unscented transformation. At each iteration, the UKF generates a set of sampling points, called sigma points, to approximate the probability distribution of the states and parameters. These sigma points can be easily transferred through the nonlinear equations, and the output sigma points are used to update the states and parameters. This gradient-free propagation scheme is remarkably attractive for parameter identification of complicated structures, for which it is usually difficult to evaluate the Jacobian derivatives of system equations analytically. Another advantage of the UKF is that the UKF exhibits a higher order of accuracy than the EKF [12]. These merits have motivated research work towards application of the UKF on structural parameter identification of highly nonlinear systems [11, 13-17].

Most of the previously cited literature deals with parameter identification in the context of estimation without considering constraints. However, most model parameters of interest follow physical laws and cannot take arbitrary values. For example, stiffness values cannot be negative for a regular structure member. This fact necessitates the application of parameter constraints in the UKF identification. To meet this requirement, many approaches have been developed for the UKF with constraints. A simple but effect way to implement constraints is projecting the sigma points on the feasible domain [18]. As the weighted average of the constrained sigma points, the state and parameter estimates heuristically follow the applied constraints. However, the projected sigma points may result in an asymmetric distribution, and thus a biased estimate. Wu and Wang [19] proposed a symmetric sigma point constraining scheme to handle box constraints. Calabrese *et al.* [13] utilized this box constrained sigma point method, together with a covariance adaptation algorithm, for nonlinear structural system identification. This method preserves the symmetric distribution of the sigma points and achieves first-order accuracy of unscented transformation. Because the weighting factors are adjusted based on a linear method [20], the covariance of the constrained sigma points may not represent the covariance of the states and parameters. In addition, Tamuly *et al.* [21] adapted the idea from [22] and replaced the constrained parameters by continuous functions whose values were within the constrained bounds. As a result, the original problem is converted to a problem of estimating new parameters using the classical UKF. However, identifiability of the problem is reduced because different values of the new parameter could correspond to the same value of the original parameter.

This paper reviews and discusses in detail the aforementioned projected sigma point method and box constrained sigma point method. Following the discussion, an improved constrained sigma point method is proposed for the implementation of general constraints. In addition, the weighting factor is adjusted based on the distance between the corresponding sigma point and the estimate. In this way, the constrained sigma points can achieve second-order accuracy of unscented transformation. Besides the constrained sigma point method, this research proposes a constrained gain method, which restricts the Kalman gain rather than modifying the sigma points to ensure that the state estimates satisfy necessary constraints.

The rest of paper is organized as follows. Section 2 briefly reviews the UKF for parameter identification. Section 3 discusses different techniques for applying constraints in the UKF. Section 4 presents the parameter identification examples of a Bouc-Wen hysteretic system and a full-scale reinforced concrete structure. In the end, Section 5 provides a summary.

2 Unscented Kalman filter (UKF) for parameter identification

This section presents the UKF for structural model parameter identification. The UKF is a nonlinear variant of Kalman filter, which propagates the first two moments of states through suitably selected sigma points and corresponding weights. The UKF can be utilized for parameter identification by forming an augmented state vector $\mathbf{x} = [\mathbf{q};\ \dot{\mathbf{q}};\ \boldsymbol{\theta}]$, where the semicolons denote the concatenation of vectors. Here, $\mathbf{q}$ is the structural displacement vector, $\dot{\mathbf{q}}$ is the velocity vector, and $\boldsymbol{\theta}$ contains the parameters to be updated. The general dynamic system is governed by a nonlinear state-space equation as:

$$\dot{\mathbf{x}} = \boldsymbol{f}(\mathbf{x}, \mathbf{u}, \mathbf{w}) \tag{1}$$

where $\mathbf{u}$ is known excitation applied on the system and $\mathbf{w}$ is a zero-mean white Gaussian process noise with $\mathbb{E}[\mathbf{w}(t)\mathbf{w}^{\mathrm{T}}(t+\tau)] = \boldsymbol{\Sigma}_{\mathbf{w}}\delta(\tau)$. At time $t = k\Delta t$, the measurement $\mathbf{y}_k$ is given as:

$$\mathbf{y}_k = \boldsymbol{h}(\mathbf{x}_k, \mathbf{u}_k, \mathbf{v}_k) \tag{2}$$

where $\mathbf{v}_k$ is the zero-mean white Gaussian measurement noise with $\mathbb{E}\left[\mathbf{v}_k\mathbf{v}_{k+l}^{\mathrm{T}}\right] = \boldsymbol{\Sigma}_{\mathbf{v}}\delta_l$.

As the state-space equation and measurement equation have noises, $\mathbf{w} \in \mathbb{R}^{n_{\mathbf{w}}}$ and $\mathbf{v}_k \in \mathbb{R}^{n_{\mathbf{v}}}$, entering those equations nonlinearly, the most general formulation of the UKF concatenates the process and measurement noise with the state vector $\mathbf{x} \in \mathbb{R}^{n_{\mathbf{x}}}$ to form a further augmented state vector $\mathbf{x}^a$ with dimension $N = n_{\mathbf{x}} + n_{\mathbf{w}} + n_{\mathbf{v}}$:

$$\mathbf{x}^a = [\mathbf{x}; \mathbf{w}; \mathbf{v}] \tag{3}$$

At time $t = k\Delta t$, the estimate of the augmented state vector is:

$$\hat{\mathbf{x}}^a_{k|k-1} = \left[\hat{\mathbf{x}}^{\mathrm{T}}_{k|k-1}; \mathbf{0}; \mathbf{0}\right] \tag{4}$$

with covariance matrix:

$$\boldsymbol{\Sigma}_{\mathbf{x}^a_{k|k-1}} = \begin{bmatrix} \boldsymbol{\Sigma}_{\mathbf{x}_{k|k-1}} & \mathbf{0} & \mathbf{0} \\ \mathbf{0} & \boldsymbol{\Sigma}_{\mathbf{w}} & \mathbf{0} \\ \mathbf{0} & \mathbf{0} & \boldsymbol{\Sigma}_{\mathbf{v}} \end{bmatrix} \tag{5}$$

The UKF estimation is separated into two main steps, i.e. measurement update step and time update step. Assuming by induction that the *a priori* estimate $\hat{\mathbf{x}}^a_{k|k-1}$ and its covariance matrix $\boldsymbol{\Sigma}_{\mathbf{x}^a_{k|k-1}}$ is known, $2N+1$ sigma points $\boldsymbol{x}^a_{k|k-1,i}$, $i = 0, 1, \cdots, 2N+1$, are generated as:

$$\begin{aligned}
&\boldsymbol{x}^a_{k|k-1,0} = \hat{\mathbf{x}}^a_{k|k-1} \\
&\boldsymbol{x}^a_{k|k-1,i} = \hat{\mathbf{x}}^a_{k|k-1} + \left(\sqrt{(N+\kappa)\boldsymbol{\Sigma}_{\mathbf{x}^a_{k|k-1}}}\right)_i \qquad i = 1,2,\cdots,N \\
&\boldsymbol{x}^a_{k|k-1,N+i} = \hat{\mathbf{x}}^a_{k|k-1} - \left(\sqrt{(N+\kappa)\boldsymbol{\Sigma}_{\mathbf{x}^a_{k|k-1}}}\right)_i \qquad i = 1,2,\cdots,N
\end{aligned} \tag{6}$$

where $\sqrt{\cdot}$ is the matrix square root and $(\cdot)_i$ refers to the i-th column of the matrix. κ is a scaling parameter, and can be any number as long as $N+\kappa>0$ [23]. The $2N+1$ weighting coefficients for the sigma points are given as:

$$\begin{aligned}
&W_0 = \frac{\kappa}{N+\kappa} \\
&W_i = \frac{1}{2(N+\kappa)} \qquad i = 1,2,\cdots,2N
\end{aligned} \tag{7}$$

Using $\boldsymbol{x}^a_{k|k-1,i} = \left[\boldsymbol{x}^{\mathbf{x}}_{k|k-1,i};\ \boldsymbol{x}^{\mathbf{w}}_{k|k-1,i};\ \boldsymbol{x}^{\mathbf{v}}_{k|k-1,i}\right]$, the predicted measurement $\boldsymbol{y}_{k|k-1,i}$ of each sigma point can be evaluated as:

$$\boldsymbol{y}_{k|k-1,i} = \boldsymbol{h}\left(\boldsymbol{x}^{\mathbf{x}}_{k|k-1,i}, \mathbf{u}_k, \boldsymbol{x}^{\mathbf{v}}_{k|k-1,i}\right) \qquad i = 0,1,\cdots,2N \tag{8}$$

The predicted measurement $\hat{\mathbf{y}}_{k|k-1}$ of state $\mathbf{x}_k$ is calculated as the weighted average of the predicted measurements of sigma points:

$$\hat{\mathbf{y}}_{k|k-1} = \sum_{i=0}^{2N} W_i \boldsymbol{y}_{k|k-1,i} \tag{9}$$

The innovation covariance matrix $\boldsymbol{\Sigma}_{\mathbf{y}_{k|k-1}}$ can be evaluated as:

$$\boldsymbol{\Sigma}_{\mathbf{y}_{k|k-1}} = \sum_{i=0}^{2N} W_i \left(\boldsymbol{y}_{k|k-1,i} - \hat{\mathbf{y}}_{k|k-1}\right)\left(\boldsymbol{y}_{k|k-1,i} - \hat{\mathbf{y}}_{k|k-1}\right)^{\mathrm{T}} \tag{10}$$

From the sigma points and the predicted measurements of sigma points, the cross covariance between the *a priori* estimate $\hat{\mathbf{x}}_{k|k-1}$ and its measurement $\hat{\mathbf{y}}_{k|k-1}$ can be calculated as:

$$\boldsymbol{\Sigma}_{\mathbf{xy}_{k|k-1}} = \sum_{i=0}^{2N} W_i \left(\boldsymbol{x}^{\mathbf{x}}_{k|k-1,i} - \hat{\mathbf{x}}_{k|k-1}\right)\left(\boldsymbol{y}_{k|k-1,i} - \hat{\mathbf{y}}_{k|k-1}\right)^{\mathrm{T}} \tag{11}$$

According to state estimation theory [23], the Kalman gain matrix is calculated as:

$$\mathbf{L}_k = \boldsymbol{\Sigma}_{\mathbf{xy}_{k|k-1}} \left(\boldsymbol{\Sigma}_{\mathbf{y}_{k|k-1}}\right)^{-1} \tag{12}$$

After measurement $\mathbf{y}_k$ is available, the measurement residual is obtained:

$$\mathbf{r}_k = \mathbf{y}_k - \hat{\mathbf{y}}_{k|k-1} \tag{13}$$

The *a posteriori* estimate $\hat{\mathbf{x}}_{k|k}$ is calculated using the Kalman gain matrix $\mathbf{L}_k$ as:

$$\hat{\mathbf{x}}_{k|k} = \hat{\mathbf{x}}_{k|k-1} + \mathbf{L}_k \mathbf{r}_k \tag{14}$$

Along with the measurement update of the state, the covariance matrix $\boldsymbol{\Sigma}_{\mathbf{x}_{k|k}}$ for the *a posteriori* estimate can be evaluated as:

$$\boldsymbol{\Sigma}_{\mathbf{x}_{k|k}} = \boldsymbol{\Sigma}_{\mathbf{x}_{k|k-1}} - \mathbf{L}_k \boldsymbol{\Sigma}_{\mathbf{y}_{k|k-1}} \mathbf{L}_k^{\mathrm{T}} \tag{15}$$

In the time update step, $2N+1$ sigma points $\boldsymbol{\mathcal{X}}_{k|k,i}^{a}$, $i = 0, 1, \cdots, 2N+1$, are generated again using updated covariance matrix $\boldsymbol{\Sigma}_{\mathbf{x}_{k|k}^{a}}$ as:

$$\begin{aligned}
&\boldsymbol{\mathcal{X}}_{k|k,0}^{a} = \hat{\mathbf{x}}_{k|k}^{a} \\
&\boldsymbol{\mathcal{X}}_{k|k,i}^{a} = \hat{\mathbf{x}}_{k|k}^{a} + \left(\sqrt{(N+\kappa)\boldsymbol{\Sigma}_{\mathbf{x}_{k|k}^{a}}}\right)_i \qquad i = 1, 2, \cdots, N \\
&\boldsymbol{\mathcal{X}}_{k|k,N+i}^{a} = \hat{\mathbf{x}}_{k|k}^{a} - \left(\sqrt{(N+\kappa)\boldsymbol{\Sigma}_{\mathbf{x}_{k|k}^{a}}}\right)_i \qquad i = 1, 2, \cdots, N
\end{aligned} \tag{16}$$

The corresponding weighting factors W_i, $i = 0, 1, \cdots, 2N$, are the same as those in Eq. (7). Using $\boldsymbol{\mathcal{X}}_{k|k,i}^{a} = \left[\boldsymbol{\mathcal{X}}_{k|k,i}^{\mathbf{x}};\ \boldsymbol{\mathcal{X}}_{k|k,i}^{\mathbf{w}};\ \boldsymbol{\mathcal{X}}_{k|k,i}^{\mathbf{v}}\right]$, each sigma point propagates through the nonlinear system to perform the time update:

$$\boldsymbol{\mathcal{X}}_{k+1|k,i}^{\mathbf{x}} = \boldsymbol{\mathcal{X}}_{k|k,i}^{\mathbf{x}} + \int_{k\Delta t}^{(k+1)\Delta t} \boldsymbol{f}\left(\boldsymbol{\mathcal{X}}_{k|k,i}^{\mathbf{x}}, \mathbf{u}, \boldsymbol{\mathcal{X}}_{k|k,i}^{\mathbf{w}}\right) dt \qquad i = 0, 1, \cdots, 2N \tag{17}$$

The *a priori* estimate $\hat{\mathbf{x}}_{k+1|k}$ can be calculated as the weighted average of the sigma points:

$$\hat{\mathbf{x}}_{k+1|k} = \sum_{i=0}^{2N} W_i \boldsymbol{\mathcal{X}}_{k+1|k,i}^{\mathbf{x}} \tag{18}$$

The corresponding covariance matrix $\boldsymbol{\Sigma}_{\mathbf{x}_{k+1|k}}$ can be evaluated as:

$$\boldsymbol{\Sigma}_{\mathbf{x}_{k+1|k}} = \sum_{i=0}^{2N} W_i \left(\boldsymbol{x}_{k+1|k,i}^{\mathbf{x}} - \hat{\mathbf{x}}_{k+1|k} \right) \left(\boldsymbol{x}_{k+1|k,i}^{\mathbf{x}} - \hat{\mathbf{x}}_{k+1|k} \right)^{\mathrm{T}} \tag{19}$$

Repeating Eq. (6) ~ Eq. (19), UKF can recursively update the system states for a nonlinear system.

3 Constrained UKF (CUKF)

Incorporating constraints in the UKF is of critical importance to reliable estimation, especially for system parameter identification. In this section, we describe several methods to incorporate constraints during the UKF identification process. Section 3.1 and Section 3.2 review the projected sigma point method and the box constrained sigma point method, respectively. Section 3.3 proposes an improved constrained sigma point method, which retains both the mean and covariance of the state distribution. In Section 3.4, a constrained gain method is discussed.

3.1 Projected sigma point method [18]

This section introduces the projected sigma point method to implement constraints in the UKF. The basic strategy of this method is to project the sigma points on the feasible domain. The projected sigma points are utilized to calculate the state estimate and covariance matrix. Figure 1 illustrates this method using a 2D example where the state estimate $\hat{\mathbf{x}}$ and covariance matrix $\Sigma_{\mathbf{x}}$ are listed as follows:

$$\hat{\mathbf{x}} = \begin{bmatrix} 1 \\ 1 \end{bmatrix} \qquad \Sigma_{\mathbf{x}} = \begin{bmatrix} 2 & 0.5 \\ 0.5 & 1 \end{bmatrix} \tag{20}$$

In Figure 1, the state estimate is denoted as the blue star sign, and the state covariance is represented by the blue dash line. Based on the state estimate and covariance, five sigma points are generated, denoted as blue diamond sign. The feasible domain in this illustration is $\boldsymbol{\Omega} = \{(x_1, x_2) \in \mathbb{R}^2 | x_1 \geq 0, x_2 \geq 0, x_1 + x_2 \leq 3\}$, which can be represented by the triangle in the figure. It is shown that three original sigma points $\boldsymbol{x}_1$, $\boldsymbol{x}_2$, and $\boldsymbol{x}_3$ fail to satisfy the constraints. These points are projected onto the boundary of the feasible domain, and are denoted as red square

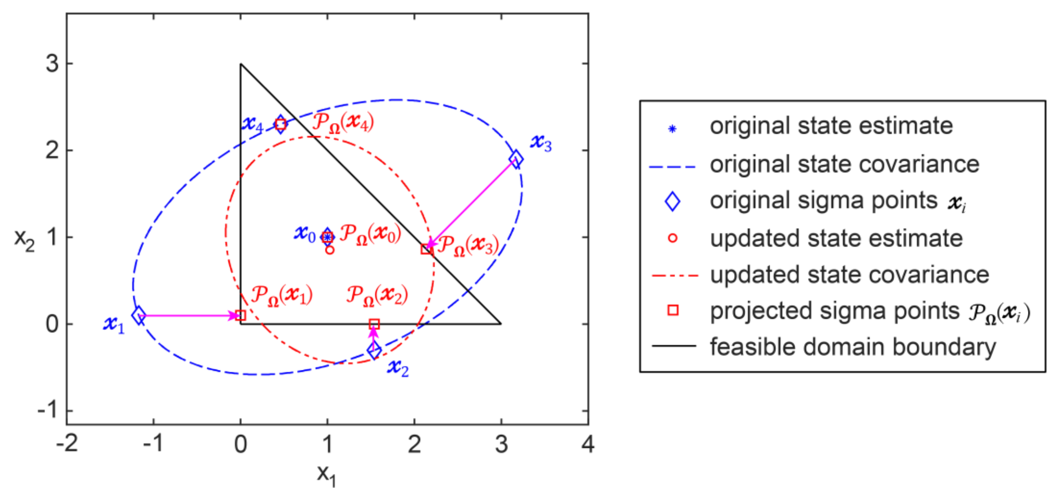

Figure 1 Illustration of the projected sigma point method

signs $\mathcal{P}_{\mathbf{\Omega}}(\boldsymbol{x}_i)$. Based on the projected sigma points, the state estimate and covariance are updated, denoted as the red circle sign and red double dot line, respectively.

When a general constraint $\boldsymbol{g}(\mathbf{x}) \geq 0$ is imposed on the system, the projection $\mathcal{P}_{\mathbf{\Omega}}$ of the original sigma point $\boldsymbol{x}_i$ on feasible domain $\mathbf{\Omega}$ can be computed by solving the following optimization problem:

$$\begin{aligned} \underset{\mathbf{x}}{\text{minimize}} \quad & \|\mathbf{x} - \boldsymbol{x}_i\|_2^2 \\ \text{subject to} \quad & \boldsymbol{g}(\mathbf{x}) \geq 0 \end{aligned} \tag{21}$$

where $\|\cdot\|_2$ denotes the ℓ_2-norm. For some special cases, analytical solutions can be obtained [24].

1. Single scalar linear inequality $\mathbf{a}^{\mathrm{T}}\mathbf{x} \geq b$, i.e. $g(\mathbf{x}) = \mathbf{a}^{\mathrm{T}}\mathbf{x} - b$

$$\mathcal{P}_{\mathbf{\Omega}}(\boldsymbol{x}_i) = \begin{cases} \boldsymbol{x}_i - (\mathbf{a}^{\mathrm{T}}\boldsymbol{x}_i - b)\mathbf{a}/\|\mathbf{a}\|_2^2 & \text{if } \mathbf{a}^{\mathrm{T}}\boldsymbol{x}_i < b \\ \boldsymbol{x}_i & \text{if } \mathbf{a}^{\mathrm{T}}\boldsymbol{x}_i \geq b \end{cases} \tag{22}$$

2. Box constraints $\mathbf{x}_{\mathrm{L}} \leq \mathbf{x} \leq \mathbf{x}_{\mathrm{U}}$ (the sign “≤” is overloaded to represent entry-wise inequality) , i.e. $\boldsymbol{g}(\mathbf{x}) = \begin{Bmatrix} \mathbf{x} - \mathbf{x}_{\mathrm{L}} \\ \mathbf{x}_{\mathrm{U}} - \mathbf{x} \end{Bmatrix}$

$$\mathcal{P}_{\mathbf{\Omega}}(\boldsymbol{x}_i)_j = \begin{cases} (\mathbf{x}_{\mathbf{L}})_j & \text{if } (\boldsymbol{x}_i)_j \leq (\mathbf{x}_{\mathbf{L}})_j \\ (\boldsymbol{x}_i)_j & \text{if } (\mathbf{x}_{\mathbf{L}})_j \leq (\boldsymbol{x}_i)_j \leq (\mathbf{x}_{\mathbf{U}})_j \\ (\mathbf{x}_{\mathbf{U}})_j & \text{if } (\boldsymbol{x}_i)_j \geq (\mathbf{x}_{\mathbf{U}})_j \end{cases} \tag{23}$$

The projection of sigma points needs to be applied in both the measurement update step Eq. (6) and time update step Eq. (16). Note that even using the projected sigma points, the *a posteriori* estimate $\hat{\mathbf{x}}_{k|k}$ obtained from Eq. (14) may not necessarily follow the constraints. In such case, the same projection method Eq. (21) can be applied on the *a posteriori* estimate $\hat{\mathbf{x}}_{k|k}$.

The projected sigma point method is simple but effective to implement constraints in the UKF. As shown in Figure 1, the projected sigma points are not necessarily symmetric around the state estimate $\hat{\mathbf{x}}$. In addition, such sigma points may not capture the mean and covariance of the system state. As shown in the above example, the updated state estimate and covariance differ from the original ones, even though the original state estimate satisfies the applied constraints.

3.2 Box constrained sigma point method [19]

This section introduces the box constrained sigma point method, which can handle the box constraints:

$$\mathbf{x}_{\mathrm{L}} \leq \mathbf{x} \leq \mathbf{x}_{\mathrm{U}} \tag{24}$$

Similar to the projected sigma point method, the box constrained sigma point method implements constraints on the sigma points during the UKF process. Rather than being projected on the feasible domain i.e. Eq.(21), the sigma points outside of the feasible domain are moved back onto the boundary along the direction to the estimate. Meanwhile, the counterpart sigma points are moved correspondingly so that the new set of sigma points remain symmetric. In the measurement update step, the sigma points are generated based on the distance d_i and direction $\left(\sqrt{\boldsymbol{\Sigma}_{\mathbf{x}}}\right)_i$ to the state estimate $\hat{\mathbf{x}}$:

$$
\begin{aligned}
&\boldsymbol{x}_0 = \hat{\mathbf{x}} & & \\
&\boldsymbol{x}_i = \hat{\mathbf{x}} + d_i\left(\sqrt{\boldsymbol{\Sigma}_{\mathbf{x}}}\right)_i & & i = 1, 2, \cdots, N \\
&\boldsymbol{x}_i = \hat{\mathbf{x}} - d_i\left(\sqrt{\boldsymbol{\Sigma}_{\mathbf{x}}}\right)_i & & i = 1, 2, \cdots, N
\end{aligned} \tag{25}
$$

where

$$
\begin{aligned}
&d_i = \min\left(\sqrt{N+\kappa}, d_i^1, d_i^2\right) \\
&d_i^1 = \min_{j=1,2,\cdots,N} \left|(\mathbf{x}_{\mathrm{U}})_j - (\hat{\mathbf{x}})_j\right| / \left|\left(\sqrt{\boldsymbol{\Sigma}_{\mathbf{x}}}\right)_{i,j}\right| \\
&d_i^2 = \min_{j=1,2,\cdots,N} \left|(\mathbf{x}_{\mathrm{L}})_j - (\hat{\mathbf{x}})_j\right| / \left|\left(\sqrt{\boldsymbol{\Sigma}_{\mathbf{x}}}\right)_{i,j}\right|
\end{aligned} \tag{26}
$$

The weighting factors of the sigma points are modified according to a linear method with respect to the distance d_i to the state estimate.

$$
\begin{aligned}
&W_0 = b & & \\
&W_i = a \cdot d_i + b & & i = 1, 2, \cdots, 2N
\end{aligned} \tag{27}
$$

where

$$
\begin{aligned}
&s = 2\sum_{i=1}^{N} d_i \\
&a = \frac{2\kappa - 1}{2(N+\kappa)\left(s - (2N+1)\sqrt{N+\kappa}\right)} \\
&b = \frac{1}{2(N+\kappa)} - \frac{2\kappa - 1}{2\sqrt{N+\kappa}\left(s - (2N+1)\sqrt{N+\kappa}\right)}
\end{aligned} \tag{28}
$$

In the time update step, the sigma points can be constrained in the same way. Note that, similar to the projected sigma point method, even using the constrained sigma points, the *a posteriori* estimate $\hat{\mathbf{x}}_{k|k}$ obtained from Eq. (14) may not necessarily satisfy the constraints. In such case, the projection method Eq. (21) can be applied on the *a posteriori* estimate $\hat{\mathbf{x}}_{k|k}$.

Figure 2 illustrates the box constrained sigma point method using a 2D example where the state estimate $\hat{\mathbf{x}}$ and covariance matrix $\Sigma_{\mathbf{x}}$ are the same as in Eq. (20). The feasible domain is set as $\boldsymbol{\Omega} = \{(x_1, x_2) \in \mathbb{R}^2 | 0 \leq x_1 \leq 3, 0 \leq x_2 \leq 3\}$, which can be represented by the rectangular in the figure. It is shown that three sigma points $\boldsymbol{x}_1$, $\boldsymbol{x}_2$, and $\boldsymbol{x}_3$ are out of the boundary. The new set of sigma points $\mathcal{C}_{\Omega}(\boldsymbol{x}_i)$ is denoted as red square sign. As shown in the figure, although the original sigma point $\boldsymbol{x}_4$ locates within the feasible domain, this sigma point is moved accordingly as the counterpart sigma point $\boldsymbol{x}_2$ is moved to the boundary. In this way, the new set of sigma points remain symmetric. Based on the new sigma points, the state estimate and covariance are updated, denoted as the red circle sign and red double dot line, respectively.

As illustrated in the figure, the new set of sigma points maintains a symmetric distribution so that the updated state estimate equals to the original state estimate. However, as the weighing factors are modified using a linear method as per Eq. (27), the updated state covariance is different from the original state covariance. Furthermore, the box constrained sigma point method can only address box constraints, which limits the application of this method.

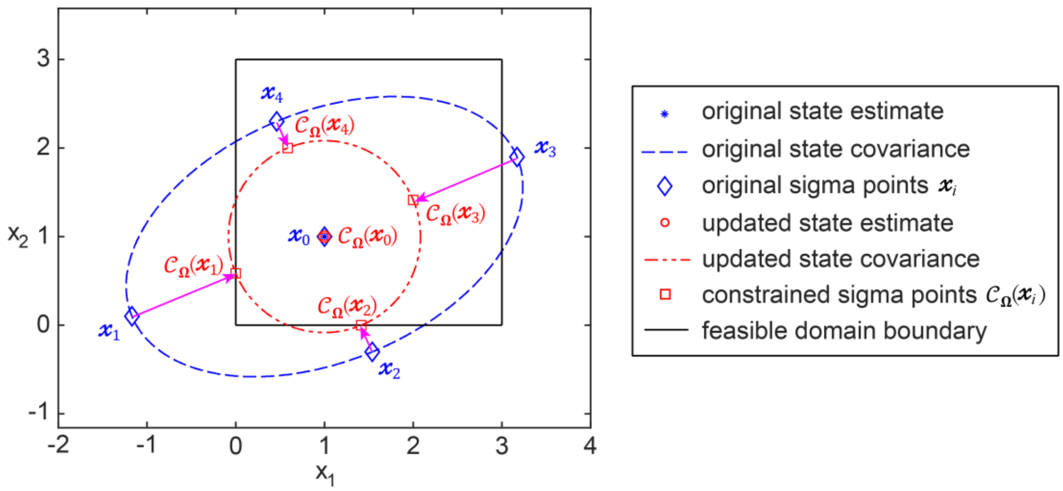

Figure 2 Illustration of the box constrained sigma point method

3.3 General constrained sigma point method

This section covers the general constrained sigma point method for the UKF. This method improves the box constrained sigma point method in two aspects. First, this method proposes a way to modify the weighting factors, based on which the new set of sigma points can retain both the mean and covariance of the state distribution. Secondly, this method can handle general constraints $\boldsymbol{g}(\mathbf{x}) \geq \mathbf{0}$ in an efficient way.

The sigma points together with corresponding weighting factors determine their statistic properties. The general constrained sigma point method still adopts Eq. (25) and Eq. (26) to adjust all the sigma points to be within the feasible domain. The determination of weighting factors is changed as follows:

$$
\begin{aligned}
W_i &= \frac{1}{2d_i^2} \qquad\qquad i = 1, 2, \cdots, 2N \\
W_0 &= 1 - \sum_{i=1}^{2N} W_i
\end{aligned}
\tag{29}
$$

It can be easily proved that the weighted mean and covariance of the sigma points match the first two moments of the original state distribution (Appendix 1). Although the proposed method enjoys this desirable property, it should be noted that if the state estimate is close to the boundary, some weighting factors may grow too large and cause numerical difficulty for application.

When the state variables encounter general constraints $\boldsymbol{g}(\mathbf{x}) \geq \mathbf{0}$ rather than box constraints, it is usually difficult to find the analytical solution to the distance between the constrained sigma points and the state estimate. Here we propose a simple but effective backtracking line search method to handle general constraints. A scaling factor $\alpha \in (0,1)$ is first chosen.

Algorithm – *Backtracking line search*

Given constraints $\boldsymbol{g}(\mathbf{x}) \geq \mathbf{0}$, state estimate $\hat{\mathbf{x}}^a_{k|k-1}$, direction $\left(\sqrt{\boldsymbol{\Sigma}_\mathbf{x}}\right)_i$, dimension N, and scalar factors κ, $\alpha \in (0,1)$

Initialize $d_i = \sqrt{N+\kappa}$

1. `while` $\boldsymbol{g}\left(\hat{\mathbf{x}}^a_{k|k-1} + d_i\left(\sqrt{\boldsymbol{\Sigma}_\mathbf{x}}\right)_i\right) < \mathbf{0}$ `or` $\boldsymbol{g}\left(\hat{\mathbf{x}}^a_{k|k-1} - d_i\left(\sqrt{\boldsymbol{\Sigma}_\mathbf{x}}\right)_i\right) < \mathbf{0}$, $d_i \coloneqq \alpha d_i$

2. **output** $\boldsymbol{x}^a_{k|k-1,i} = \hat{\mathbf{x}}^a_{k|k-1} + d_i\left(\sqrt{\boldsymbol{\Sigma}_\mathbf{x}}\right)_i$, $\boldsymbol{x}^a_{k|k-1,i+N} = \hat{\mathbf{x}}^a_{k|k-1} - d_i\left(\sqrt{\boldsymbol{\Sigma}_\mathbf{x}}\right)_i$

The backtracking line search starts with $d_i = \sqrt{N+\kappa}$, and keeps reducing it by the scaling factor α until both the sigma points $\boldsymbol{x}^a_{k|k-1,i}$ and $\boldsymbol{x}^a_{k|k-1,i+N}$ satisfy the constraints. The scaling factor is often chosen to be between 0.1 and 0.8, where 0.1 corresponds to a very crude search and 0.8 corresponds to a finer search [24].

Figure 3 illustrates the constrained sigma point method using a 2D example where the state estimate $\hat{\mathbf{x}}$ and covariance matrix $\Sigma_\mathbf{x}$ are the same as in Eq. (20). A nonlinear constraint is required on the state:

$$\left(\mathbf{x} - \begin{bmatrix}1\\1\end{bmatrix}\right)^{\mathrm{T}} \begin{bmatrix}2 & -0.5\\-0.5 & 1\end{bmatrix}^{-1} \left(\mathbf{x} - \begin{bmatrix}1\\1\end{bmatrix}\right) < 1 \tag{30}$$

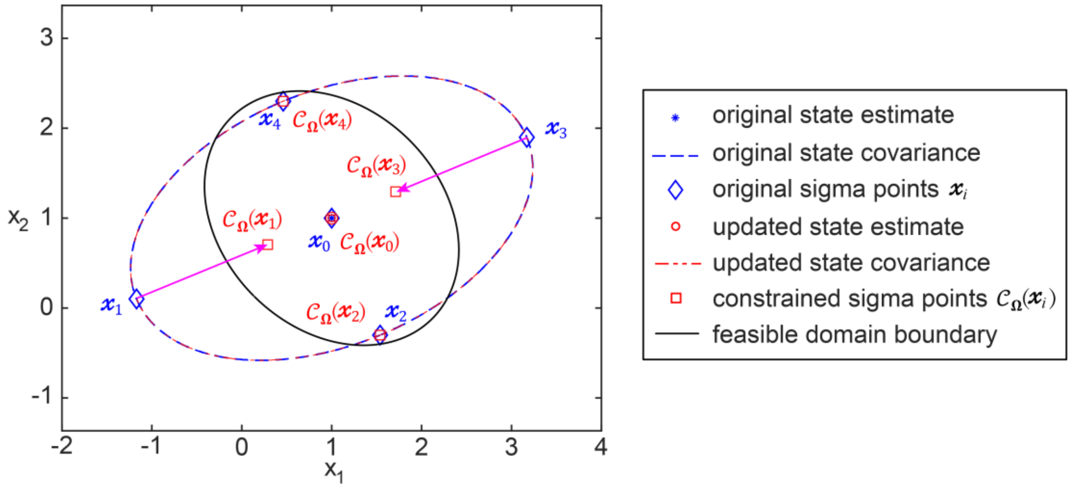

Figure 3 Illustration of the general constrained sigma point method

The feasible domain $\boldsymbol{\Omega}$ can be represented by the region inside the black eclipse in Figure 3. It is shown that two sigma points are out of the boundary. The new set of sigma points is denoted as red square sign. Based on the new sigma points, the state estimate and covariance are updated, denoted as the red circle sign and red double dot line, respectively.

In this example, the scaling factor is chosen to be 0.8. As the backtracking line search is inexact, the constrained sigma points do not locate on the boundary of the feasible domain but within it. Furthermore, it can be observed that both the updated state estimate and covariance are the same as the original ones.

3.4 Constrained gain method

This section describes the constrained gain method for the UKF. Instead of modifying the sigma points, the UKF can apply constraints by modifying the Kalman gain. Such idea has been investigated for state estimation using Kalman filter [25] and parameter identification using EKF [26]. The Kalman gain $\mathbf{L}_k$ at time $t = k\Delta t$ of the unconstrained UKF (Eq. (12)) can be analytically solved by minimizing the trace of *a posteriori* state covariance matrix (Eq. (A.4)):

$$\underset{\mathbf{L}}{\text{minimize}}\ \text{Trace}\left(\boldsymbol{\Sigma}_{\mathbf{x}_{k|k-1}} - \boldsymbol{\Sigma}_{\mathbf{xy}_{k|k-1}}\mathbf{L}^{\mathrm{T}} - \mathbf{L}\boldsymbol{\Sigma}_{\mathbf{yx}_{k|k-1}} + \mathbf{L}\boldsymbol{\Sigma}_{\mathbf{y}_{k|k-1}}\mathbf{L}^{\mathrm{T}}\right) \tag{31}$$

When general constraints $\boldsymbol{g}(\mathbf{x}) \geq \mathbf{0}$ are imposed on the system, the Kalman gain of the constrained UKF can be numerically calculated by solving the optimization problem:

$$\begin{aligned}&\underset{\mathbf{L}}{\text{minimize}}\ \text{Trace}\left(\boldsymbol{\Sigma}_{\mathbf{x}_{k|k-1}} - \boldsymbol{\Sigma}_{\mathbf{xy}_{k|k-1}}\mathbf{L}^{\mathrm{T}} - \mathbf{L}\boldsymbol{\Sigma}_{\mathbf{yx}_{k|k-1}} + \mathbf{L}\boldsymbol{\Sigma}_{\mathbf{y}_{k|k-1}}\mathbf{L}^{\mathrm{T}}\right)\\ &\text{subject to}\ \boldsymbol{g}\left(\hat{\mathbf{x}}_{k|k-1} + \mathbf{L}\left(\mathbf{y}_k - \hat{\mathbf{y}}_{k|k-1}\right)\right) \geq \mathbf{0}\end{aligned} \tag{32}$$

The optimal solution $\mathbf{L}^*$ ensures that the *a posteriori* estimates $\hat{\mathbf{x}}_{k|k} = \hat{\mathbf{x}}_{k|k-1} + \mathbf{L}^*\left(\mathbf{y}_k - \hat{\mathbf{y}}_{k|k-1}\right)$ are guaranteed to satisfy the constraints $\boldsymbol{g}\left(\hat{\mathbf{x}}_{k|k}\right) \geq \mathbf{0}$. Meanwhile, the corresponding covariance matrix $\boldsymbol{\Sigma}_{\mathbf{x}_{k|k}}$ can also be calculated using $\mathbf{L}^*$ in Eq. (15).

If affine constraints $\mathbf{Ax} - \mathbf{b} \geq \mathbf{0}$ are needed on the state variables, the analytical solution to the optimization problem Eq. (32) can be derived. Here, $\mathbf{A} \in \mathbb{R}^{n_c \times n_x}$ is a constant coefficient matrix and $\mathbf{b} \in \mathbb{R}^{n_c}$ is a constant coefficient vector. Consider the *i*-th constraint in $\mathbf{Ax} - \mathbf{b} \geq \mathbf{0}$, which is simply a scalar inequality $g_i(\mathbf{x}) = \mathbf{a}_i^{\mathrm{T}}\mathbf{x} - b_i \geq 0, i = 1,2, \dots, n_c$. For a feasible $\mathbf{x}$, the constraint is said to be *active* if the equal sign holds, i.e. $\mathbf{a}_i^{\mathrm{T}}\mathbf{x} = b_i$; the constraint is said to be *inactive* if the strict greater-than relationship $\mathbf{a}_i^{\mathrm{T}}\mathbf{x} - b_i > 0$ holds [24]. At time $t = k\Delta t$, suppose that n_{ac} of the n_c inequality constraints are active. Denote by $\mathbf{A}_{\mathrm{a}} \in \mathbb{R}^{n_{ac} \times n_x}$ the full-ranked n_{ac} rows of $\mathbf{A}$ that correspond to the active constraints, and denote by $\mathbf{b}_{\mathrm{a}} \in \mathbb{R}^{n_{ac}}$ the n_{ac} entries of $\mathbf{b}$ that correspond to the active constraints. The optimization problem to compute the Kalman gain $\mathbf{L}$ with equality constraint $\mathbf{A}_{\mathrm{a}}\mathbf{x} - \mathbf{b}_{\mathrm{a}} = \mathbf{0}$ is formulated as:

$$\begin{aligned}&\underset{\mathbf{L}}{\text{minimize}}\ \text{Trace}\left(\boldsymbol{\Sigma}_{\mathbf{x}_{k|k-1}} - \boldsymbol{\Sigma}_{\mathbf{xy}_{k|k-1}}\mathbf{L}^{\mathrm{T}} - \mathbf{L}\boldsymbol{\Sigma}_{\mathbf{yx}_{k|k-1}} + \mathbf{L}\boldsymbol{\Sigma}_{\mathbf{y}_{k|k-1}}\mathbf{L}^{\mathrm{T}}\right)\\ &\text{subject to}\ \mathbf{A}_{\mathrm{a}}\left(\hat{\mathbf{x}}_{k|k-1} + \mathbf{L}\left(\mathbf{y}_k - \hat{\mathbf{y}}_{k|k-1}\right)\right) - \mathbf{b}_{\mathrm{a}} = \mathbf{0}\end{aligned} \tag{33}$$

The Kalman gain matrix $\tilde{\mathbf{L}}_k$ and the *a posteriori* estimate $\tilde{\mathbf{x}}_{k|k}$ of the unconstrainted UKF are given by Eq. (12) and Eq. (14), respectively.

$$\tilde{\mathbf{L}}_k = \mathbf{\Sigma}_{\mathbf{xy}_{k|k-1}} \left(\mathbf{\Sigma}_{\mathbf{y}_{k|k-1}}\right)^{-1} \tag{34}$$

$$\tilde{\mathbf{x}}_{k|k} = \hat{\mathbf{x}}_{k|k-1} + \tilde{\mathbf{L}}_k \mathbf{r}_k \tag{35}$$

Under mild assumptions, the solution of this equality constrained optimization problem is given as:

$$\mathbf{L}_k = \tilde{\mathbf{L}}_k - \mathbf{A}_\mathrm{a}^\mathrm{T}(\mathbf{A}_\mathrm{a}\mathbf{A}_\mathrm{a}^\mathrm{T})^{-1}\left(\mathbf{A}_\mathrm{a}\tilde{\mathbf{x}}_{k|k} - \mathbf{b}_\mathrm{a}\right)\left(\mathbf{r}_k^\mathrm{T}\mathbf{\Sigma}_{\mathbf{y}_k}^{-1}\mathbf{r}_k\right)^{-1}\mathbf{r}_k^\mathrm{T}\mathbf{\Sigma}_{\mathbf{y}_k}^{-1} \tag{36}$$

Using this Kalman gain, the *a posteriori* estimate $\hat{\mathbf{x}}_{k|k}$ of constrained UKF is found to be related to the unconstrained UKF estimate $\tilde{\mathbf{x}}_{k|k}$:

$$\hat{\mathbf{x}}_{k|k} = \tilde{\mathbf{x}}_{k|k} - \mathbf{A}_\mathrm{a}^\mathrm{T}(\mathbf{A}_\mathrm{a}\mathbf{A}_\mathrm{a}^\mathrm{T})^{-1}\left(\mathbf{A}_\mathrm{a}\tilde{\mathbf{x}}_{k|k} - \mathbf{b}_\mathrm{a}\right) \tag{37}$$

The general constrained gain method is applied only in the measurement update step. At the expense of increasing computational complexity, the *a posteriori* estimate is promised to satisfy the constraints. In addition, the analytical solution to the inequality constrained system can significantly accelerate the estimation process. Furthermore, without modifying sigma points, this method keeps the first two moments of the system state, which is a desirable property for reliable estimation.

4 Application

To evaluate the performance of the various constraining approaches in Section 3, parameter identification using simulation and experiment data is conducted. Section 4.1 presents parameter identification of a Bouc-Wen hysteretic system. Section 4.2 investigates the performance of constrained UKF through experimental data collected from a full-scale reinforced concrete frame structure.

4.1 Bouc-Wen hysteretic system

The Bouc-Wen model has been extensively used to describe the hysteresis phenomenon of various types of structures, including magnetorheological (MR) dampers and beam-column joints. Consider a single degree of freedom (SDOF) Bouc-Wen hysteretic model subject to earthquake excitation, as shown in Figure 4. The dynamic equation of this hysteretic system with mass m, damping coefficient c, stiffness k and ground excitation $\ddot{q}_g$ is shown as:

$$m\ddot{q}(t) + c\dot{q}(t) + kz(t) = -m\left(\ddot{q}_g(t) + w(t)\right) \tag{38}$$

Here the excitation to the system is $u = -m\ddot{q}_g(t)$, and the ground acceleration $\ddot{q}_g(t)$ is contaminated with zero-mean white Gaussian process noise with $\mathbb{E}[w(t)w(t+\tau)] = \Sigma_w\delta(\tau)$. The nonlinear restoring force is $r(t) = kz(t)$, and z is a hidden hysteretic displacement. A first-order differential equation describes the hysteretic displacement:

$$\dot{z} = \dot{q}\left(1 - |z|^n\left(\gamma + \beta \operatorname{sgn}(z\dot{q})\right)\right) \tag{39}$$

Here β, γ, and n are dimensionless parameters controlling the shape and magnitude of the hysteresis loop; $\operatorname{sgn}(\cdot)$ is the signum function.

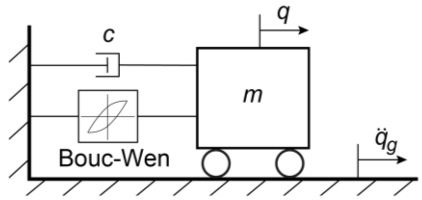

Figure 4 Bouc-Wen hysteretic system

In this simulation example, system parameters are set as $m = 1$ kg, $c = 0.3$ Ns/m, $k = 12$ N/m, $\beta = 2$, $\gamma = 1$, and $n = 2$. The parameters to be identified are c, k, β, γ, and n, while the mass m is treated as known. A scaled El Centro earthquake of 40 s duration is adopted as the ground excitation. The state-space system equation for parameter identification can be formulated as:

$$\mathbf{x} = \begin{pmatrix} q \\ \dot{q} \\ z \\ c \\ k \\ \beta \\ \gamma \\ n \end{pmatrix} \qquad \dot{\mathbf{x}} = \boldsymbol{f}\left(\mathbf{x}, \ddot{q}_g, w\right) = \begin{pmatrix} \dot{q} \\ -\left(\ddot{q}_g + w\right) - (c\dot{q} + kz)/m \\ \dot{q}\left(1 - |z|^n\left(\gamma + \beta \operatorname{sgn}(z\dot{q})\right)\right) \\ 0 \\ 0 \\ 0 \\ 0 \\ 0 \end{pmatrix} \tag{40}$$

Figure 5 plots the excitation $\ddot{q}_g$ and simulated responses including displacement q, velocity $\dot{q}$, hysteretic displacement z, and the hysteretic loop of the SDOF Bouc-Wen hysteretic system.

To identify both the system states and parameters, the absolute acceleration of the mass block is measured at $t = k\Delta t$ and the measurement equation is given as:

$$y_k = -(c\dot{q}_k + kz_k)/m + v_k \tag{41}$$

Here v_k is zero-mean white Gaussian process noise with $\mathbb{E}[v_k v_{k+l}] = \Sigma_v \delta_l$ contaminating the measurement results.

Inequality constraints applied on the parameters are listed as follows:

$$c \geq 0, \qquad k \geq 0, \qquad \beta + \gamma \geq 0, \qquad \beta - \gamma \geq 0, \qquad n \geq 1 \tag{42}$$

All the constrained UKF methods described in Section 3, together with the unconstrained UKF, are used to identify the Bouc-Wen model parameters. As the linear inequality constraints cannot be directly implemented in the box constrained sigma point method, the backtracking line search introduced in Section 3.3 is applied to find the suitable distance between the sigma points and the state estimate.

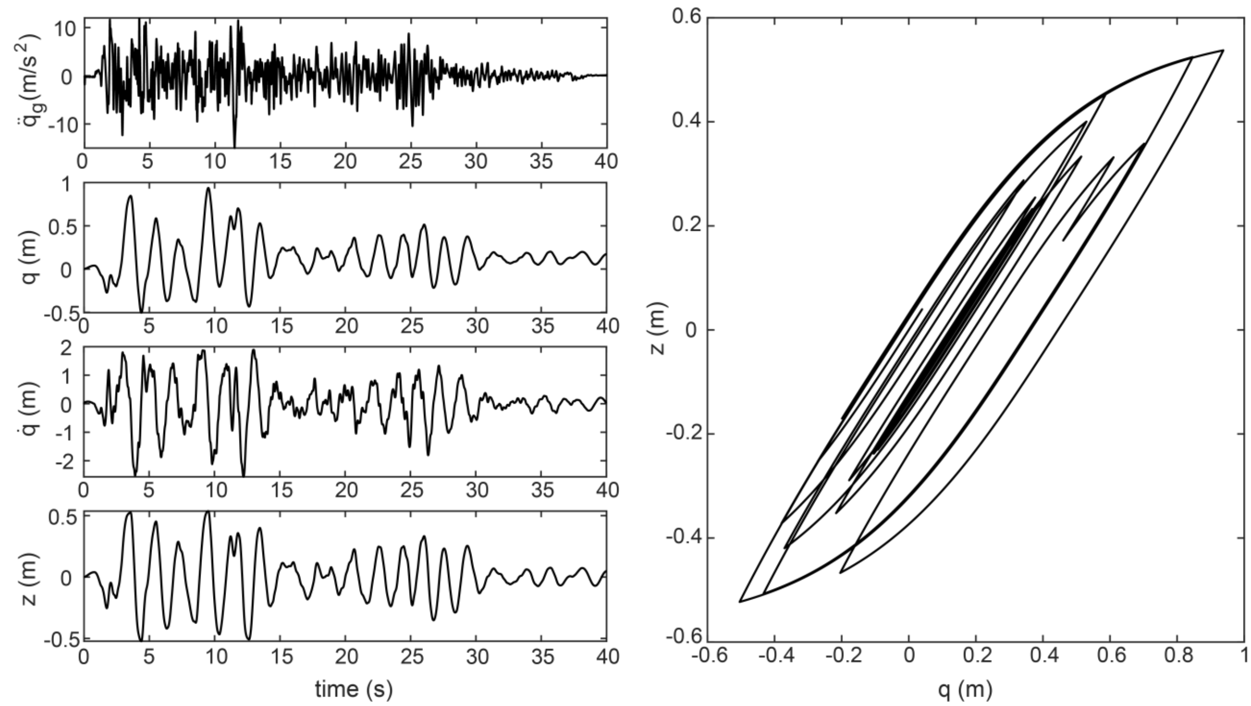

Figure 5 Excitation and dynamic responses of the hysteretic system

4.1.1 Strictly feasible initial estimate

In the first simulation, the initial parameter estimates are set as $c_{0|-1} = 0.15$ Ns/m, $k_{0|-1} = 6$ N/m, $\beta_{0|-1} = 1$, $\gamma_{0|-1} = 0.5$, and $n_{0|-1} = 4$, which strictly satisfy the constraints. The covariance of the process noise is set as $\Sigma_w = (10^{-2}\ \mathrm{m/s^2})^2$, and the covariance of measurement noise is set as $\Sigma_v = (10^{-2}\ \mathrm{m/s^2})^2$. To study the parameter identification performance of the constrained UKF methods, 100 independent runs of simulation are performed, each of which is conducted using randomly generated process noise and measurement noise.

The run #1 is chosen as the example to show the time histories of the *a posteriori* estimates of the parameters (Figure 6). The results show that all the methods, including the unconstrained UKF, can recursively update all the parameters from their initial values to the corresponding true values. It can be observed from the close-up plot Figure 6(b) that the estimates of stiffness parameter k and damping coefficient c converge faster than the estimates of hysteretic parameters, which remain not updated within the first 1.5 seconds. The reason is that at the beginning of vibration, the structure has not exhibited nonlinear behavior. After about 4 seconds, all the estimates reach values quite close to the true values. For this example, the unconstrained UKF, the general constrained sigma point method, and the constrained gain method perform nearly the same. On the other hand, the projected sigma point method and the box constrained sigma point method have slightly larger estimation error during the first 4 seconds, especially for hysteretic parameters. This difference is caused by the fact that the sigma points of these two methods cannot represent the first two moments of the states and parameters.

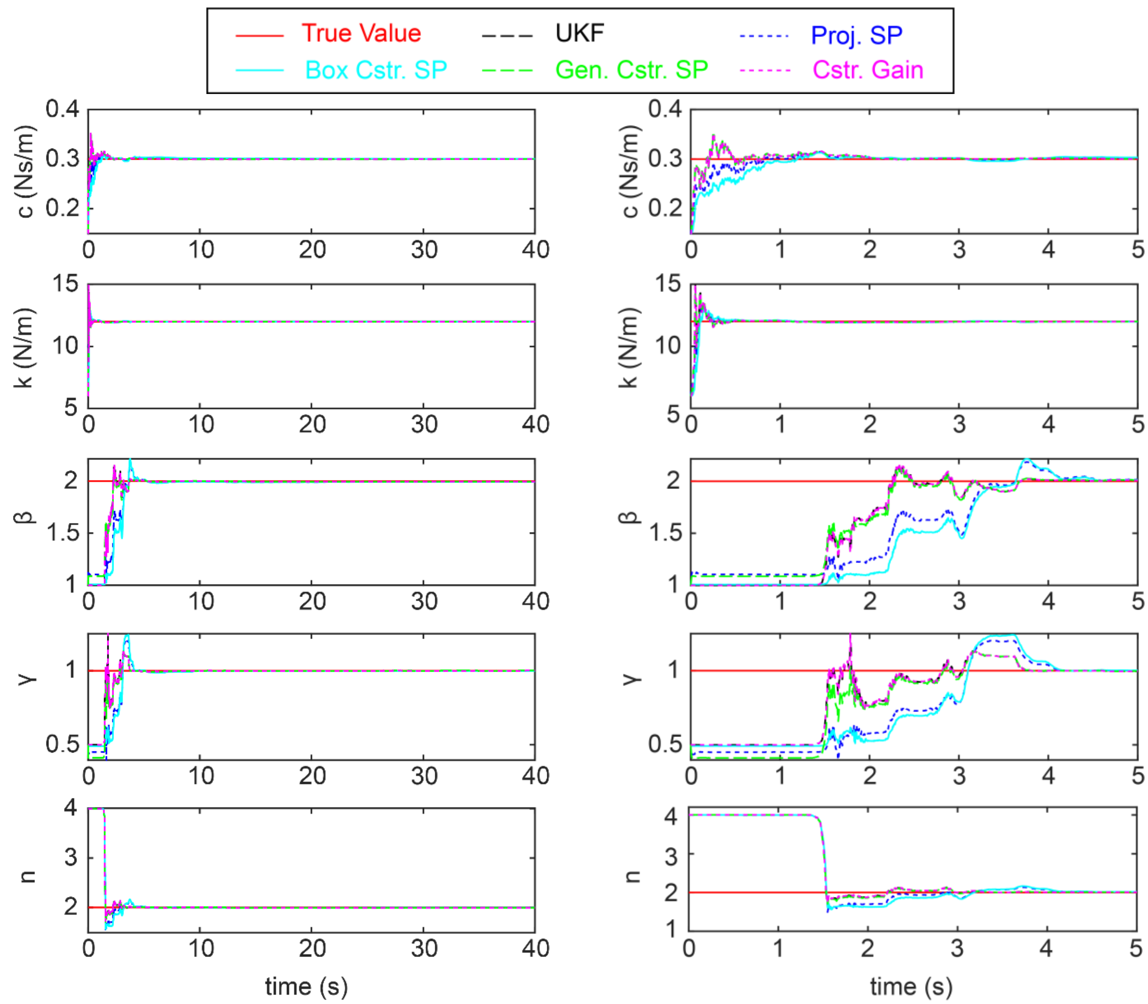

(a) Entire time span (b) Close-up (0 ~ 5 s)

Figure 6 Parameter identification results using strictly feasible initial estimate

Table 1 summarizes the averaged estimation errors at the end of identification process from the 100 simulation runs on the Bouc-Wen model. The results indicate that using the strictly feasible initial estimate, all the constrained UKF methods can identify model parameters with acceptable accuracy. All estimation errors are less than 0.3%. Generally, the estimation errors of the

Table 1 Averaged estimation errors using strictly feasible initial estimate (%)

Parameters	UKF	Proj. SP	Box Cstr. SP	Cstr. SP	Cstr. Gain
c	0.0698	0.1956	0.2516	0.0815	0.0704
k	0.0104	0.0163	0.0178	0.0107	0.0103
β	0.1430	0.1670	0.1797	0.1435	0.1429
γ	0.1501	0.2253	0.2709	0.1507	0.1507
n	0.0834	0.0921	0.0801	0.0865	0.0833

unconstrained UKF, the constrained sigma point method, and the constrained gain method are less than the errors of the other two methods.

4.1.2 Marginally feasible initial estimate

In the second simulation, the initial parameter estimates are set as $c_{0|-1} = 0.15$ Ns/m, $k_{0|-1} = 6$ N/m, $\beta_{0|-1} = 0.5$, $\gamma_{0|-1} = 0.5$, and $n_{0|-1} = 4$, which marginally satisfy the constraint $\beta - \gamma \geq 0$. This initial setting increases challenge for the parameter estimation, as a small perturbation may result in an infeasible estimate. Based on the same process noise and measurement noise covariance in Section 4.1.1, 100 independent runs of simulation are performed.

The run #1 is chosen as the example to show the time histories of the *a posteriori* estimates of the parameters using the marginally feasible initial estimate (Figure 7). In this scenario, the identification results of the projected sigma point method slightly differ from the true parameter values. Except for the stiffness parameter k, all the other parameters cannot be updated correctly by the box constrained sigma point method. On the other hand, the general constrained sigma point method, which adopts the same backtracking line search but adjusts the weighting factors to retain

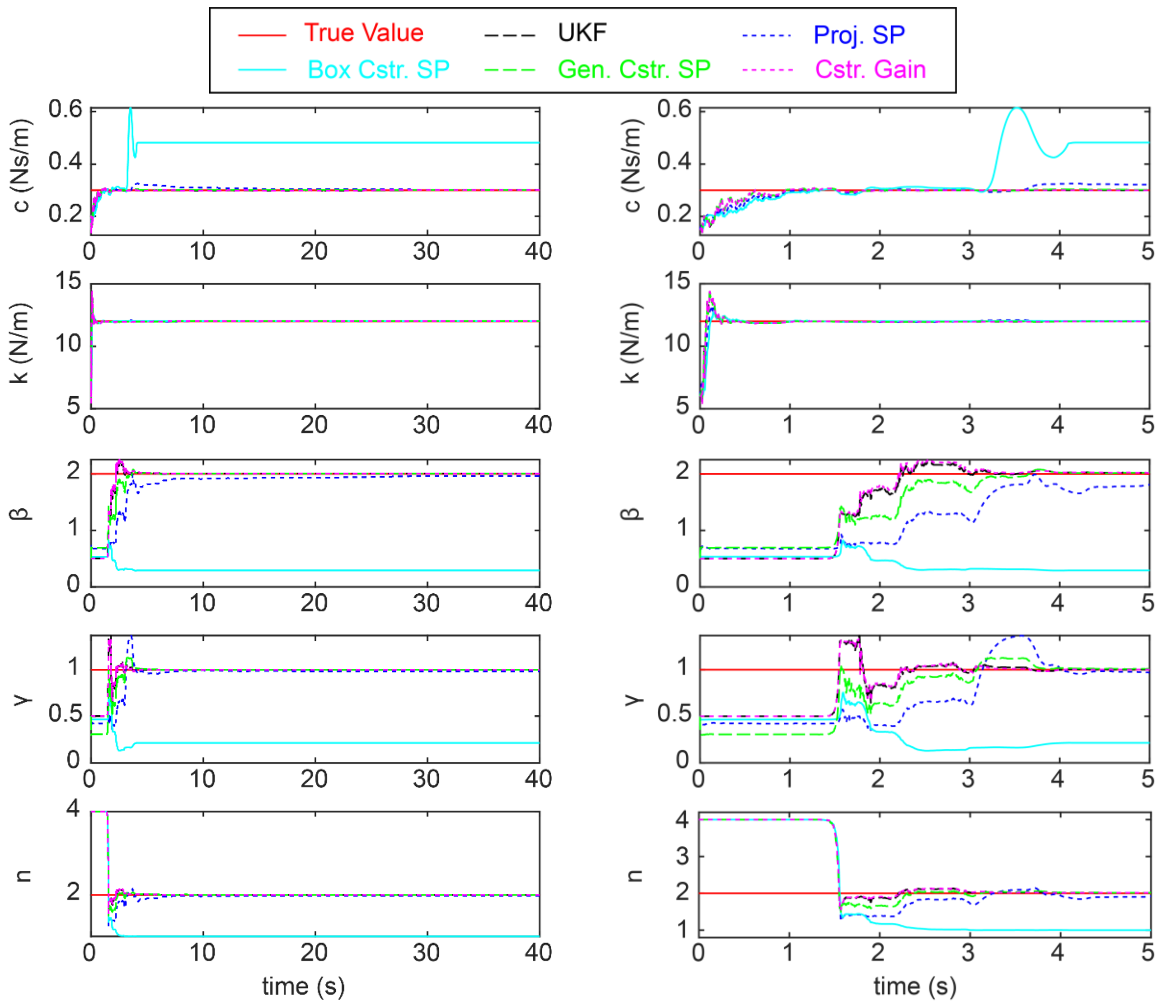

(a) Entire time span (b) Close-up (0 ~ 5 s)

Figure 7 Parameter identification results using marginally feasible initial estimate the state covariance, can provide reliable identification results for all parameters. In addition, the unconstrained UKF and the constrained gain method can recursively update all the parameters from their initial values to the corresponding true values.

Table 2 summarizes the averaged estimation errors at the end of identification process from the 100 simulation runs on the Bouc-Wen model. Compared to the strictly feasible initial estimate, the marginally feasible initial estimate causes more errors in the parameter identification results. The least reliable method for this scenario is the box constrained sigma point method, which can only update the stiffness parameters correctly. The projected sigma point method performs better but identification errors of hysteretic parameters are greater than 5%. The constrained sigma point method provides more reliable identification results, with all errors are less than 5%. It is interesting that the unconstrained UKF can identify the model parameters with errors less than 1%. The constrained gain method performs the best and all the identification errors are less than 0.5%.

Table 2 Averaged estimation errors using marginally feasible initial estimate (%)

Parameters	UKF	Proj. SP	Box Cstr. SP	Cstr. SP	Cstr. Gain
c	0.1371	4.2143	46.3022	0.9263	0.1073
k	0.0200	0.8691	0.6412	0.5000	0.0130
β	0.5658	12.2363	77.5621	4.6934	0.3118
γ	0.5545	6.7312	66.5106	2.6362	0.2675
n	0.3323	5.5192	48.1743	3.0070	0.1636

In this example, the unconstrained UKF outperforms the methods adjusting sigma points and only the constrained gain method provides slightly better identification results than the unconstrained UKF. The reasons are described as follows. First, during the identification process, estimates by the unconstrained UKF happen to satisfy the constraints most of the time, even though the generated sigma points occasionally violate the constraints. Other researchers [11] also found in their examples that the unconstrained UKF could accurately identify hysteretic parameters without implementing constraints on the sigma points. Second, compared to the unconstrained UKF, the constrained gain method is less aggressive and prevents the *a posteriori* estimate from violating the constraints by restricting Kalman gain. Thus, when the unconstrained UKF performs well, the constrained gain method should perform well too; on the other hand, when the unconstrained UKF provides an unreasonable estimate, the constrained gain method utilizes a smaller gain in the measurement update and prevents the estimate from violating the constraints. Last but not least, all the other methods implement constraints by adjusting the sigma points, even when the estimate does not violate the constraints.

In addition, besides adjusting the sigma points, the projected sigma point method changes both the mean and covariance of system state (as illustrated in Figure 1), while the box constrained sigma point method keeps the mean but changes the covariance of system state (as illustrated in Figure 2). The modification of the state's statistical properties could introduce more uncertainties and contribute to the large identification errors, as shown in Figure 7(b) and Table 2. As for the constrained sigma point method, although both mean and covariance are preserved, this method effectively puts much higher weight on the adjusted sigma points than those satisfying constraints, because the weight is inversely proportional to the distance square d_i^2 (Eq. (29) and Figure 3). This is somewhat counterintuitive as an originally good sigma point gets a lower weight but an adjusted sigma point gets a higher weight. As a result, the constrained sigma point method performs similarly as the unconstrained UKF and the constrained gain method when the initial setting is less challenging (Figure 6) but causes a larger error when the initial setting is more challenging (Figure 7).

4.2 Full scale concrete frame structure

Four reinforced concrete frames were constructed and tested in the Structural Engineering and Materials Laboratory on Georgia Tech campus, as shown in Figure 8(a). The four frames are separate from each other, with a gap between every two neighboring frames. Each frame consists of two stories and two bays with a total height of 24 ft and a total length of 36 ft. When testing each frame, a 75-kip hydraulic linear inertial shaker was installed on the second elevated slab and utilized to excite the frame with a scaled El Centro record. The moving mass of the shaker can provide in-plane excitation along longitudinal direction. Experimental measurements from the frame #1 are used in this research. When constructing the frame, concrete was poured in five stages. Figure 8(b) illustrates the pour sequence for the frame.

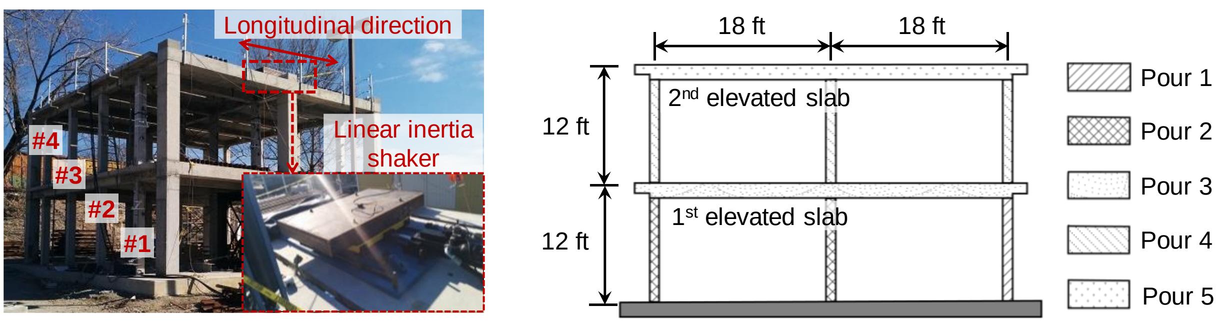

(a) Reinforced concrete frame (b) Sequence of construction

Figure 8 Full-scale test frame and pour sequence

A total of 44 in-plane acceleration channels were installed to measure the dynamical responses of the concrete frame. Figure 9 illustrates the sensor instrumentation, including 27 channels along longitudinal direction (annotated by blue arrows) and 17 channels along vertical direction (annotated by red arrows). These sensors were installed at mid-length and quarter-length of each beam or column member. The sampling frequency was set as 200 Hz.

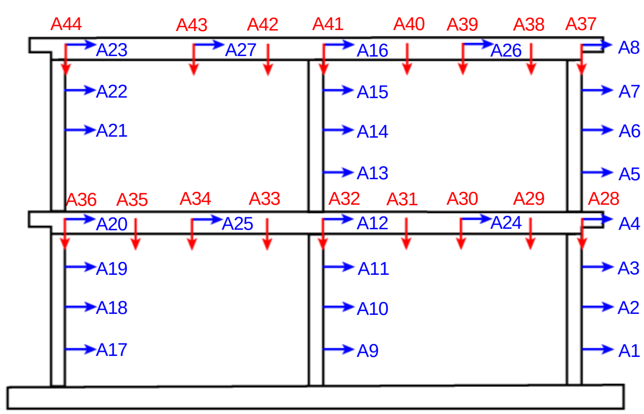

Figure 9 Sensor instrumentation

Figure 10 plots two sets of example acceleration data collected by accelerometers A16 and A18, together with the corresponding frequency spectra. The response spectra indicate that the motion of the structure due to shaker excitation is significant in frequency range from 0 ~ 10 Hz, while higher frequency components also exist.

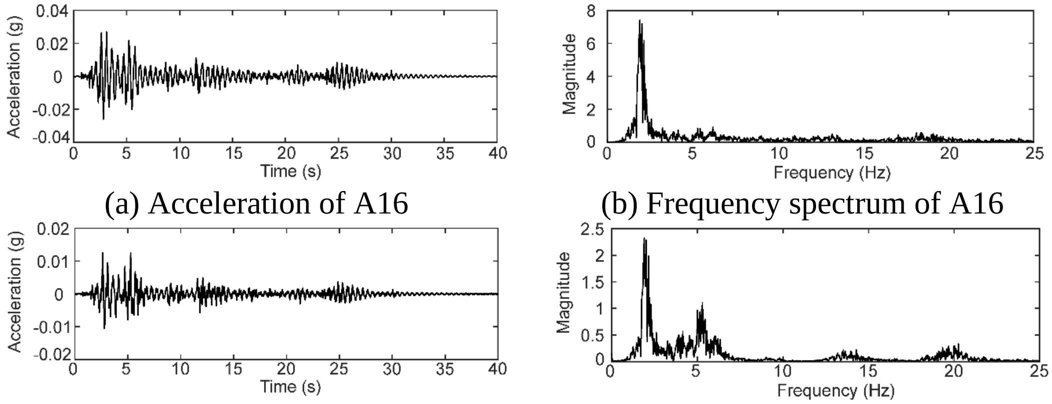

(a) Acceleration of A16 (b) Frequency spectrum of A16

(c) Acceleration of A18 (d) Frequency spectrum of A18

Figure 10 Full-scale test frame and pour sequence

A 2D FE model for the reinforced concrete frame is built using Euler-Bernoulli beam elements as shown in Figure 11. The model consists of 23 nodes, 24 elements, and 36 DOFs in total. Axial deformations of beam elements are neglected in this model. The three bases are modelled as fixed end. Composite sections are adopted to consider the contribution from both concrete and rebars. According to the sensor instrumentation and the finite element model, it is assumed that 15 DOFs are measured by sensors, as shown in Figure 11.

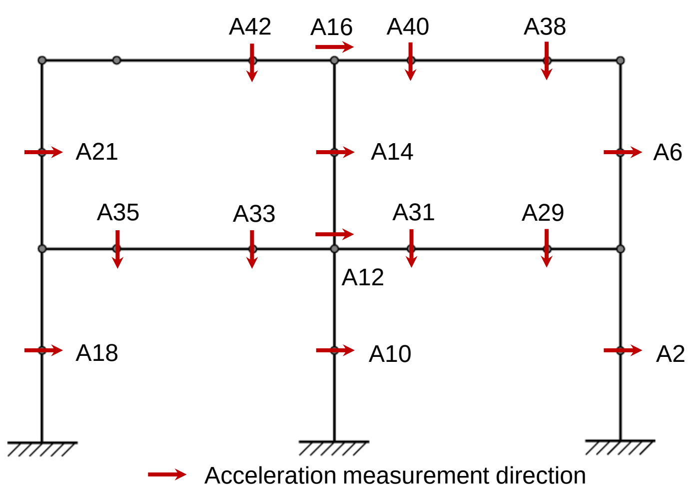

Figure 11 FE model for the reinforced concrete frame

Table 3 Nominal values of Young’s moduli of concrete and steel (Unit: kips/in^2)

Material	Young’s moduli
Concrete	3,800
Steel	28,000

Table 3 summarizes the nominal values of Young's moduli of the concrete and steel rebars for the initial model.

Five stiffness variables $\boldsymbol{\theta} \in \mathbb{R}^5$ corresponding to the five concrete pours (Figure 8(b)) are selected for updating. For the structural members constructed during the i-th pour, variable θ_i represents the relative change of the actual Young's modulus value (to be identified) from the nominal value in Table 3. Besides five stiffness variables $\boldsymbol{\theta} \in \mathbb{R}^5$, two damping ratios $\boldsymbol{\zeta} \in \mathbb{R}^2$ are also updated for constructing a Rayleigh damping matrix. To improve the computational efficiency, Guyan model reduction technique [27] is applied to condense the FE model to the 15 measured DOFs. Based on the condensed model, the dynamical responses are calculated through Newmark-beta method. The initial estimates are set as $\theta_{i,0|-1} = 0$ and $\zeta_{i,0|-1} = 0.02$. Inequality constraints of the model parameters are listed as follows:

$$-0.3 \leq \theta_i \leq 0.3, \qquad\qquad 0.001 \leq \zeta_i \leq 0.2 \tag{43}$$

Considering its robustness, only the CUKF using constrained gain method is conducted and compared with the unconstrained UKF. Figure 12 plots the time histories of the *a posteriori* parameter estimates of the reinforced concrete frame structure using the UKF and the CUKF on experimental data. The stiffness variables and damping ratios start updating from the beginning of vibration. After the significant change during the beginning 5 s, the parameter estimates gradually converge to constant values. It should be noted that estimates generated from the CUKF always stay within the feasible domain, while some estimates from the UKF violate the constraints during

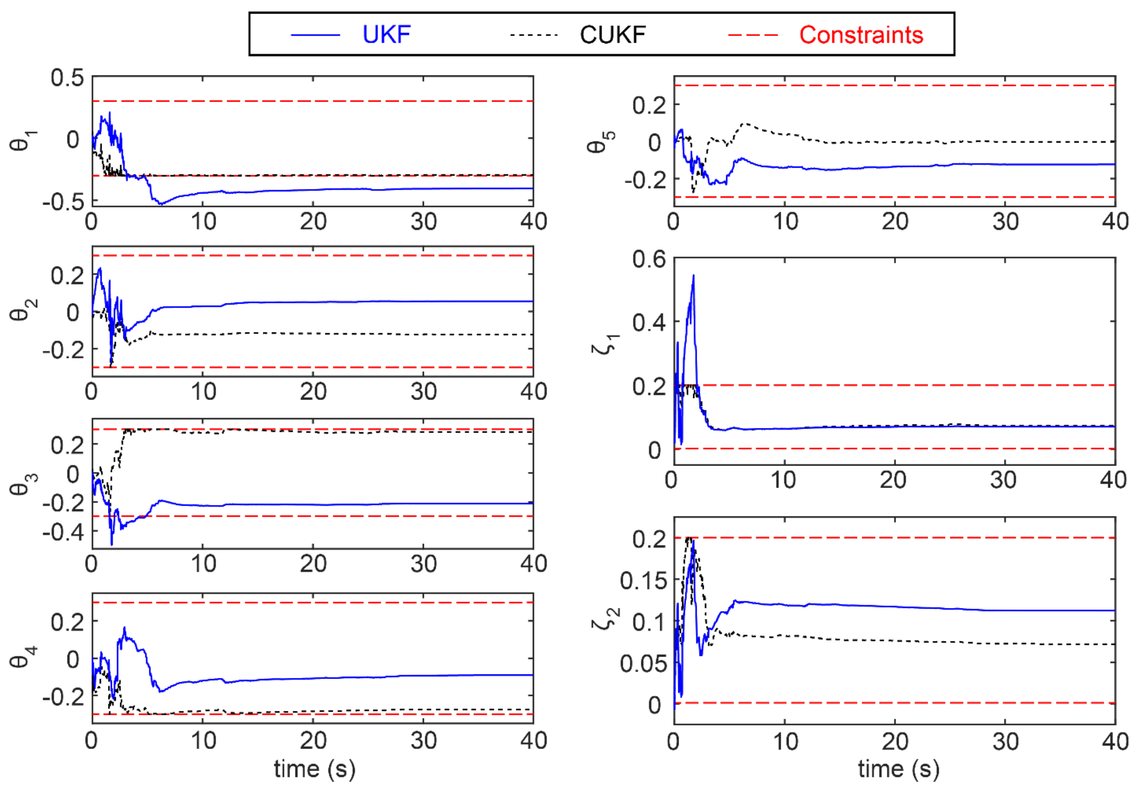

Figure 12 Identified stiffness variables and damping ratios from UKF and CUKF using experimental data

the identification process. For example, the UKF estimate of θ_1 decreases below -0.3 after about 5 s, and the UKF estimate ζ_1 grows above 0.2 at the beginning of estimation. Except for ζ_1, the UKF and the CUKF provide different identification results for the model parameters.

Table 4 summarizes the identification results provided by the UKF and the CUKF for the reinforced concrete frame structure using experimental data. Both the UKF and the CUKF results show that the stiffness values of members constructed by the 1^{st}, 4^{th} and 5^{th} concrete pours decrease from the nominal value. However, the UKF and the CUKF provide opposite changes on the stiffness values of members constructed by the 2^{nd} and 3^{rd} concrete pours. The decrease in stiffness values of column members (θ_1, θ_2 and θ_4) can be caused by the P-Δ effect. In this sense, the CUKF identification results of stiffness parameters are more reasonable than the UKF results. The damping ratios identified by the CUKF are reasonable for reinforced concrete structures, whose damping ratios typically range from 0.05 to 0.10 [28]. On the other hand, the UKF provides a reasonable value for ζ_1 but ζ_2 is higher than the normal expected range.

Table 4 Identification results using the UKF and the CUKF of the reinforced concrete frame structure using experimental data

Parameters	UKF	CUKF
θ_1	-0.4045	-0.2931
θ_2	0.0542	-0.1236
θ_3	-0.2127	0.2803
θ_4	-0.0913	-0.2746
θ_5	-0.1236	-0.0021
ζ_1	0.0696	0.0736
ζ_2	0.1122	0.0720

Based on the parameter identification results from the UKF and CUKF, updated FE models are built. The dynamical responses of the reinforced concrete frame structure are simulated using the same excitation. Figure 13 plots the simulated acceleration responses of the frame structure at

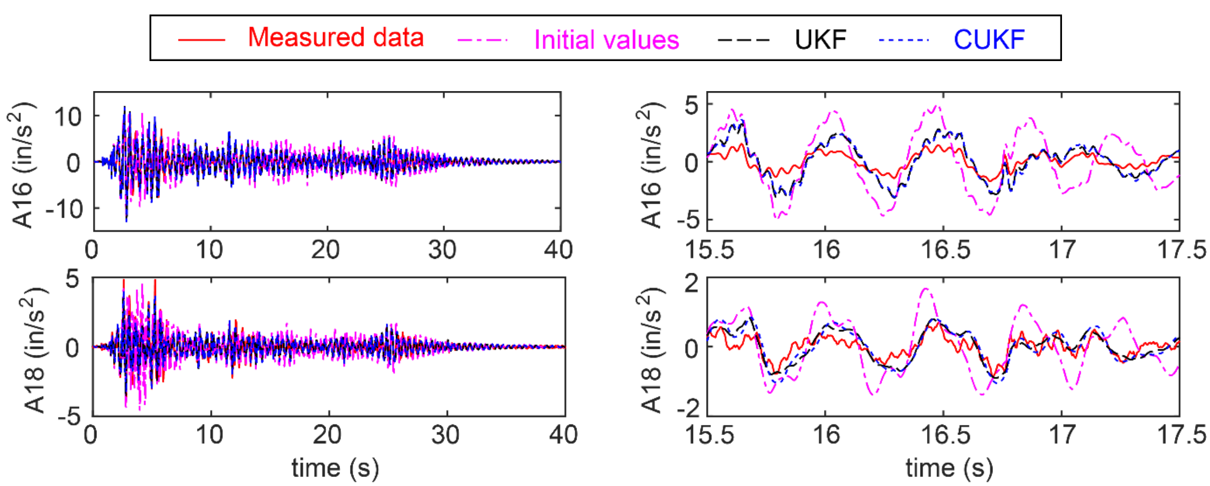

(a) Entire time span (b) Close-up (15.5 ~ 17.5 s)

Figure 13 Simulated acceleration using initial model parameters and parameters updated by the UKF and CUKF location A16 and A18 using initial model parameters and the updated parameter values from the UKF and CUKF algorithms. Acceleration responses of entire time span from 0 s to 40 s are plotted in Figure 13(a). The close-up plots of 15.5 s to 17.5 s are shown in Figure 13(b). The comparison shows that both the UKF and CUKF identified parameters provide acceleration responses close to measurement data, while initial model parameters cannot generate accurate acceleration response.

To quantify the performance of the UKF and CUKF, Table 5 summarizes the root mean square (RMS) errors of the simulated acceleration responses for the entire 40 s time span. Compared with the initial FE model, both the UKF and CUKF updated FE models provide simulated responses with less RMS errors. With the help of applied constraints, the CUKF performs slightly better than the UKF. It also should be emphasized that although FE models updated by the UKF and the CUKF provide similar dynamic responses, the parameters identified by the CUKF are more reasonable in the engineering sense.

Table 5 RMS error comparison of simulated acceleration responses of updated models from the UKF and CUKF (Unit: in/s^2)

Channel	Initial	UKF	CUKF	Channel	Initial	UKF	CUKF
A2	0.7727	0.3516	0.3413	A29	0.1734	0.1425	0.1384
A6	1.5568	0.7475	0.7507	A31	0.0455	0.0500	0.0322
A10	0.8014	0.3454	0.3322	A33	0.0536	0.0377	0.0316
A12	1.3393	0.5828	0.5684	A35	0.1548	0.1434	0.1198
A14	1.5241	0.7085	0.7072	A38	0.2009	0.1358	0.1404
A16	1.9091	0.8847	0.8940	A40	0.1061	0.0594	0.0630
A18	0.7764	0.3487	0.3363	A42	0.0846	0.0437	0.0453
A21	1.5536	0.7524	0.7514				

5 Conclusion

This paper investigates parameter identification of structural systems using constrained UKF methods. Four constrained UKF methods are discussed, including the projected sigma point method, the box constrained sigma point method, the constrained sigma point method, and the constrained gain method. The first three methods implement constraints by modifying the sigma points, which either cannot retain the mean and covariance of the states or may cause numerical difficulties during application. The last method does not make any change on the sigma points but restricting the Kalman gain to ensure that the state estimates satisfy applied constraints. Simulation on an SDOF Bouc-Wen hysteretic system demonstrates that the constrained gain method is the most robust way to implement constraints in the UKF, as it can provide reliable identification results for different initial estimates. The constrained gain method is further validated through experimental measurement data of a full-scale reinforced concrete frame structure. The identification results show that incorporating constraints during the estimation process can effectively prevent the parameters from being unrealistic. In addition, all the final estimates of the constrained gain method are within reasonable range while the UKF provides unreasonably high values for some stiffness and damping parameters. The updated model parameters are used to simulate the dynamical behaviors of the reinforced concrete frame structure. The simulation results show that acceleration responses of updated models are much closer to the measured responses than the initial model. In terms of achieving smaller RMS errors, the model updated by the constrained gain method performs better than the model updated by the UKF.

Appendix

1. Weighted mean and covariance of the constrained sigma points

The sigma points and corresponding weighting factors are calculated according to Eq. (25) and Eq. (29), respectively. The weighted mean of the sigma points $\boldsymbol{x}_i$ equals to the state estimate $\hat{\mathbf{x}}$:

$$\begin{aligned}\mathbb{E}(\boldsymbol{x}) &= \sum_{i=0}^{2N} W_i \boldsymbol{x}_i \\ &= W_0 \hat{\mathbf{x}} + \sum_{i=1}^{N} W_i \left(\hat{\mathbf{x}} + d_i \left(\sqrt{\boldsymbol{\Sigma}_{\mathbf{x}}}\right)_i\right) + \sum_{i=1}^{N} W_i \left(\hat{\mathbf{x}} - d_i \left(\sqrt{\boldsymbol{\Sigma}_{\mathbf{x}}}\right)_i\right) \\ &= \hat{\mathbf{x}} \sum_{i=0}^{2N} W_i \\ &= \hat{\mathbf{x}}\end{aligned} \tag{A.1}$$

The weighted covariance of the sigma points equals to the state covariance $\boldsymbol{\Sigma}_{\mathbf{x}}$:

$$\begin{aligned}\mathbb{Cov}(\boldsymbol{x}) &= \sum_{i=0}^{2N} W_i (\boldsymbol{x}_i - \hat{\mathbf{x}})\,(\boldsymbol{x}_i - \hat{\mathbf{x}})^{\mathrm{T}} \\ &= W_0 (\hat{\mathbf{x}} - \hat{\mathbf{x}})(\hat{\mathbf{x}} - \hat{\mathbf{x}})^{\mathrm{T}} \\ &\quad + \sum_{i=1}^{N} \frac{1}{2d_i^2} \left(\hat{\mathbf{x}} + d_i \left(\sqrt{\boldsymbol{\Sigma}_{\mathbf{x}}}\right)_i - \hat{\mathbf{x}}\right) \left(\hat{\mathbf{x}} + d_i \left(\sqrt{\boldsymbol{\Sigma}_{\mathbf{x}}}\right)_i - \hat{\mathbf{x}}\right)^{\mathrm{T}} \\ &\quad + \sum_{i=1}^{N} \frac{1}{2d_i^2} \left(\hat{\mathbf{x}} - d_i \left(\sqrt{\boldsymbol{\Sigma}_{\mathbf{x}}}\right)_i - \hat{\mathbf{x}}\right) \left(\hat{\mathbf{x}} - d_i \left(\sqrt{\boldsymbol{\Sigma}_{\mathbf{x}}}\right)_i - \hat{\mathbf{x}}\right)^{\mathrm{T}} \\ &= \sum_{i=1}^{N} \left(\sqrt{\boldsymbol{\Sigma}_{\mathbf{x}}}\right)_i \left(\sqrt{\boldsymbol{\Sigma}_{\mathbf{x}}}\right)_i^{\mathrm{T}} \\ &= \boldsymbol{\Sigma}_{\mathbf{x}}\end{aligned} \tag{A.2}$$

2. Solution to the equality constrained UKF

The *a posteriori* estimate $\hat{\mathbf{x}}_{k|k}$ is calculated using the Kalman gain matrix $\mathbf{L}_k$:

$$\hat{\mathbf{x}}_{k|k} = \hat{\mathbf{x}}_{k|k-1} + \mathbf{L}_k \left(\mathbf{y}_k - \hat{\mathbf{y}}_{k|k-1}\right) \tag{A.3}$$

The *a posteriori* covariance $\boldsymbol{\Sigma}_{\mathbf{x}_{k|k}}$ is calculated as:

$$\begin{aligned}\boldsymbol{\Sigma}_{\mathbf{x}_{k|k}} &= \mathbb{E}\left[\left(\mathbf{x} - \hat{\mathbf{x}}_{k|k-1} - \mathbf{L}_k \left(\mathbf{y}_k - \hat{\mathbf{y}}_{k|k-1}\right)\right) \left(\mathbf{x} - \hat{\mathbf{x}}_{k|k-1} - \mathbf{L}_k \left(\mathbf{y}_k - \hat{\mathbf{y}}_{k|k-1}\right)\right)^{\mathrm{T}}\right] \\ &= \boldsymbol{\Sigma}_{\mathbf{x}_{k|k-1}} - \boldsymbol{\Sigma}_{\mathbf{xy}_{k|k-1}} \mathbf{L}_k^{\mathrm{T}} - \mathbf{L}_k \boldsymbol{\Sigma}_{\mathbf{yx}_{k|k-1}} + \mathbf{L}_k \boldsymbol{\Sigma}_{\mathbf{y}_{k|k-1}} \mathbf{L}_k^{\mathrm{T}}\end{aligned} \tag{A.4}$$

Consider the equality constrained optimization problem:

$$\begin{aligned}&\underset{\mathbf{L}}{\text{minimize}}\ \ \text{Trace}\left(\mathbf{\Sigma}_{\mathbf{x}_{k|k-1}}-\mathbf{\Sigma}_{\mathbf{xy}_{k|k-1}}\mathbf{L}^{\mathrm{T}}-\mathbf{L}\mathbf{\Sigma}_{\mathbf{yx}_{k|k-1}}+\mathbf{L}\mathbf{\Sigma}_{\mathbf{y}_{k|k-1}}\mathbf{L}^{\mathrm{T}}\right)\\&\text{subject to}\ \ \mathbf{A}_{\mathrm{a}}\left(\hat{\mathbf{x}}_{k|k-1}+\mathbf{L}\big(\mathbf{y}_k-\hat{\mathbf{y}}_{k|k-1}\big)\right)-\mathbf{b}_{\mathrm{a}}=\mathbf{0}\end{aligned} \tag{A.5}$$

Using Lagrange multiplier $\boldsymbol{\nu}\in\mathbb{R}^{n_{ac}}$, the Lagrangian for the problem is:

$$\begin{aligned}\mathcal{L}(\mathbf{L},\boldsymbol{\nu})= \text{Trace}&\left(\mathbf{\Sigma}_{\mathbf{x}_{k|k-1}}-\mathbf{\Sigma}_{\mathbf{xy}_{k|k-1}}\mathbf{L}^{\mathrm{T}}-\mathbf{L}\mathbf{\Sigma}_{\mathbf{yx}_{k|k-1}}+\mathbf{L}\mathbf{\Sigma}_{\mathbf{y}_{k|k-1}}\mathbf{L}^{\mathrm{T}}\right)\\&+\boldsymbol{\nu}^{\mathrm{T}}\big(\mathbf{A}_{\mathrm{a}}\big(\hat{\mathbf{x}}_{k|k-1}+\mathbf{L}\mathbf{r}_k\big)-\mathbf{b}_{\mathrm{a}}\big)\end{aligned} \tag{A.6}$$

Here $\mathbf{r}_k=\mathbf{y}_k-\hat{\mathbf{y}}_{k|k-1}$ is the measurement residual. The partial derivatives of $\mathcal{L}(\mathbf{L},\boldsymbol{\nu})$ with respect to $\mathbf{L}$ and $\boldsymbol{\nu}$, respectively, can be obtained as:

$$\frac{\partial}{\partial\mathbf{L}}\mathcal{L}(\mathbf{L},\boldsymbol{\nu})=-2\mathbf{\Sigma}_{\mathbf{xy}_{k|k-1}}+2\mathbf{L}\mathbf{\Sigma}_{\mathbf{y}_{k|k-1}}+\mathbf{A}_{\mathrm{a}}^{\mathrm{T}}\boldsymbol{\nu}\mathbf{r}_k^{\mathrm{T}} \tag{A.7}$$

$$\frac{\partial}{\partial\boldsymbol{\nu}}\mathcal{L}(\mathbf{L},\boldsymbol{\nu})=\mathbf{A}_{\mathrm{a}}\big(\hat{\mathbf{x}}_{k|k-1}+\mathbf{L}\mathbf{r}_k\big)-\mathbf{b}_{\mathrm{a}} \tag{A.8}$$

The optimality requires that both partial derivatives are zero. Assume $\mathbf{A}_{\mathrm{a}}\in\mathbb{R}^{n_{\mathrm{ac}}\times n_{\mathbf{x}}}$ is a full row-rank matrix with $\text{rank}(\mathbf{A}_{\mathrm{a}})=n_{\mathrm{ac}}\le n_{\mathbf{x}}$. Solving the equation $\frac{\partial}{\partial\mathbf{L}}\mathcal{L}(\mathbf{L},\boldsymbol{\nu})=\mathbf{0}$ for $\mathbf{L}$ provides:

$$\mathbf{L}=\mathbf{\Sigma}_{\mathbf{xy}_{k|k-1}}\mathbf{\Sigma}_{\mathbf{y}_{k|k-1}}^{-1}-\frac{1}{2}\mathbf{A}_{\mathrm{a}}^{\mathrm{T}}\boldsymbol{\nu}\mathbf{r}_k^{\mathrm{T}}\mathbf{\Sigma}_{\mathbf{y}_{k|k-1}}^{-1} \tag{A.9}$$

Substituting Eq. (A.9) into the partial derivative Eq. (A.8) and solving the equation $\frac{\partial}{\partial\boldsymbol{\nu}}\mathcal{L}(\mathbf{L},\boldsymbol{\nu})=\mathbf{0}$ for $\boldsymbol{\nu}$ provides:

$$\boldsymbol{\nu}=2(\mathbf{A}_{\mathrm{a}}\mathbf{A}_{\mathrm{a}}^{\mathrm{T}})^{-1}\left(\mathbf{A}_{\mathrm{a}}\left(\hat{\mathbf{x}}_{k|k-1}+\mathbf{\Sigma}_{\mathbf{xy}_{k|k-1}}\mathbf{\Sigma}_{\mathbf{y}_{k|k-1}}^{-1}\mathbf{r}_k\right)-\mathbf{b}_{\mathrm{a}}\right)\left(\mathbf{r}_k^{\mathrm{T}}\mathbf{\Sigma}_{\mathbf{y}_{k|k-1}}^{-1}\mathbf{r}_k\right)^{-1} \tag{A.10}$$

Finally, substituting $\boldsymbol{\nu}$ into Eq. (A.9), the Kalman gain of CUKF can be rewritten as:

$$\mathbf{L}=\tilde{\mathbf{L}}_k-\mathbf{A}_{\mathrm{a}}^{\mathrm{T}}(\mathbf{A}_{\mathrm{a}}\mathbf{A}_{\mathrm{a}}^{\mathrm{T}})^{-1}\big(\mathbf{A}_{\mathrm{a}}\tilde{\mathbf{x}}_{k|k}-\mathbf{b}_{\mathrm{a}}\big)\big(\mathbf{r}_k^{\mathrm{T}}\mathbf{\Sigma}_{\mathbf{y}_k}^{-1}\mathbf{r}_k\big)^{-1}\mathbf{r}_k^{\mathrm{T}}\mathbf{\Sigma}_{\mathbf{y}_k}^{-1} \tag{A.11}$$

Here $\tilde{\mathbf{L}}_k$ and $\tilde{\mathbf{x}}_{k|k}$ are the unconstrained Kalman gain Eq. (34) and the unconstrained *a posteriori* estimate Eq.(35), respectively.

Reference

1. Friswell, M. and J.E. Mottershead, *Finite element model updating in structural dynamics*. Vol. 38. 2013: Springer Science & Business Media.
2. Teughels, A., J. Maeck, and G. De Roeck, *Damage assessment by FE model updating using damage functions.* Computers & Structures, 2002. **80**(25): 1869-1879.

3. Friswell, M.I., *Damage identification using inverse methods.* Philosophical Transactions of the Royal Society A: Mathematical, Physical and Engineering Sciences, 2007. **365**(1851): 393-410.

4. Jeen-Shang, L. and Z. Yigong, *Nonlinear structural identification using extended Kalman filter.* Computers & Structures, 1994. **52**(4): 757-764.

5. Zhou, L., S. Wu, and J.N. Yang, *Experimental study of an adaptive extended Kalman filter for structural damage identification.* Journal of Infrastructure Systems, 2008. **14**(1): 42-51.

6. Ebrahimian, H., R. Astroza, and J.P. Conte, *Extended Kalman filter for material parameter estimation in nonlinear structural finite element models using direct differentiation method.* Earthquake Engineering & Structural Dynamics, 2015. **44**(10): 1495-1522.

7. Corigliano, A. and S. Mariani, *Parameter identification in explicit structural dynamics: performance of the extended Kalman filter.* Computer Methods in Applied Mechanics and Engineering, 2004. **193**(36-38): 3807-3835.

8. Zhang, C., et al., *Structural damage identification by extended K alman filter with l 1 -norm regularization scheme.* Structural Control and Health Monitoring, 2017. **24**(11): e1999.

9. Hoshiya, M. and E. Saito, *Structural identification by extended Kalman filter.* Journal of Engineering Mechanics, 1984. **110**(12): 1757-1770.

10. Yang, J.N., et al., *An adaptive extended Kalman filter for structural damage identification.* Structural Control and Health Monitoring, 2006. **13**(4): 849-867.

11. Wu, M. and A.W. Smyth, *Application of the unscented Kalman filter for real - time nonlinear structural system identification.* Structural Control and Health Monitoring, 2007. **14**(7): 971-990.

12. Julier, S.J. and J.K. Uhlmann. *New extension of the Kalman filter to nonlinear systems*. in *Signal processing, sensor fusion, and target recognition VI*. 1997. International Society for Optics and Photonics.

13. Calabrese, A., S. Strano, and M. Terzo, *Adaptive constrained unscented Kalman filtering for real - time nonlinear structural system identification.* Structural Control and Health Monitoring, 2018. **25**(2): e2084.

14. Chatzi, E.N., A.W. Smyth, and S.F. Masri, *Experimental application of on-line parametric identification for nonlinear hysteretic systems with model uncertainty.* Structural Safety, 2010. **32**(5): 326-337.

15. Xie, Z. and J. Feng, *Real-time nonlinear structural system identification via iterated unscented Kalman filter.* Mechanical Systems and Signal Processing, 2012. **28**: 309-322.

16. Omrani, R., R. Hudson, and E. Taciroglu, *Parametric identification of nondegrading hysteresis in a laterally and torsionally coupled building using an unscented Kalman filter.* Journal of Engineering Mechanics, 2013. **139**(4): 452-468.

17. Chatzi, E.N. and A.W. Smyth, *The unscented Kalman filter and particle filter methods for nonlinear structural system identification with non - collocated heterogeneous sensing.* Structural Control and Health Monitoring, 2009. **16**(1): 99-123.

18. Kandepu, R., B. Foss, and L. Imsland, *Applying the unscented Kalman filter for nonlinear state estimation.* Journal of Process Control, 2008. **18**(7-8): 753-768.

19. Wu, B. and T. Wang, *Model updating with constrained unscented Kalman filter for hybrid testing.* Smart Structures and Systems, 2014. **14**(6): 1105-1129.

20. Vachhani, P., S. Narasimhan, and R. Rengaswamy, *Robust and reliable estimation via unscented recursive nonlinear dynamic data reconciliation.* Journal of Process Control, 2006. **16**(10): 1075-1086.

21. Tamuly, P., A. Chakraborty, and S. Das, *Experimental verification of constrained minimum variance unbiased estimator for simultaneous input and state estimation of Bounded Input and Bounded Output (BIBO) type Bouc–Wen hysteretic structural system.* Structural Control and Health Monitoring, 2021. **28**(1): e2648.

22. Yang, Y. and F. Ma, *Constrained Kalman filter for nonlinear structural identification.* Journal of Vibration and Control, 2003. **9**(12): 1343-1357.

23. Simon, D., *Optimal state estimation: Kalman, H infinity, and nonlinear approaches*. 2006: John Wiley & Sons.

24. Boyd, S.P. and L. Vandenberghe, *Convex optimization*. 2004: Cambridge University Press.

25. Gupta, N. and R. Hauser, *Kalman filtering with equality and inequality state constraints.* arXiv preprint arXiv:0709.2791, 2007.

26. Sen, S. and B. Bhattacharya, *Online structural damage identification technique using constrained dual extended Kalman filter.* Structural Control and Health Monitoring, 2017. **24**(9): e1961.

27. Guyan, R.J., *Reduction of stiffness and mass matrices.* AIAA Journal, 1965. **3**(2): 380-380.

28. Chopra, A.K., *Dynamics of structures: Theory and applications to earthquake engineering*. Fourth ed. 2011, Upper Saddle River, NJ: Prentice Hall.